Frequency and Intensity Considerations in the Far-IR Spectroscopy of Faujasite Zeolites: Experiment and Theory. Metal Cation Vibrational Assignments, Site Locations, and Populations

Mark D. Baker, John Godber, and Geoffrey A. Ozin*

Contribution from Lash Miller Chemistry Laboratories, University of Toronto, Toronto, Ontario, Canada M5S 1A1. *Received November 26, 1984*

Abstract: A self-consistent methodology for assigning the far-IR spectra of metal-ion-exchanged faujasite zeolites is described. This approach employs a local molecule **GF**-matrix and transition-bond-dipole approximation for computing the vibrational frequencies and integrated IR intensities of cation modes for each $M^{q+}O_n$ lattice site of metal faujasite zeolites. By reference to several key alkali, alkaline-earth, and transition-metal faujasites, it is demonstrated that the combined use of the frequencies and intensities of site-specific metal cation far-IR modes allows one to secure metal cation vibrational assignments for sites I, I′, II, III′, and III″, to refine incomplete X-ray diffraction analyses, thereby providing a straightforward method for locating previously unidentified cations, and to distinguish different cations and establish cation occupancies, locations, and angles in the zeolite framework.

Molecular sieve zeolites currently play a major role in the chemical industry, acting as catalysts in a plethora of reactions as documented in recent reviews.[1,2] Among the most popular are the large-pore faujasites[3] which will be the subject of this paper. In understanding, at a fundamental level, the manner in which zeolites act as catalysts, progress depends on an array of research programs using highly sophisticated techniques. A great challenge has always been to unequivocally locate the position of cations in the zeolite framework. The main sites in the faujasite lattice where positively charged species can be immobilized are illustrated in Figure 1. Cations that are introduced into the zeolite via ion exchange clearly modify its catalytic behavior, and their location at specific sites is therefore a highly desirable goal.

Historically, X-ray diffraction techniques[4-7] both of single crystals and powders have played an important part in accumulating a data bank of zeolite framework morphology, cation site locations, and occupancies. Recently, Mortier[8] has compiled an extensive library of extra framework sites for 36 different structure types which proves to be an invaluable aid when assessing the physicochemical properties of these materials. However, the identification of cation site locations and occupancies is, except in a few cases, incomplete. This often arises from the difficulty of distinguishing between different metal cations in the zeolite. For example, in the case of MnNaY, the X-ray determination is inaccurate due to the difficulty in separating sodium and manganese ions in sites I′ and II.[9] We will return to this point later and show how far-infrared spectroscopy can be used to refine incomplete X-ray analyses.

Far-infrared spectroscopy is able to directly probe the cations immobilized in zeolites via their characteristic site vibrational modes. Recently we have shown how this technique can be used to address a number of different aspects of zeolite chemistry[10,25,26] covering such areas as catalysis, crystal field effects, the formation and growth of metal clusters in the voids of the zeolite, and deammination processes in faujasites. In this paper we will demonstrate how far-infrared spectroscopy utilizing both the frequencies and intensities of site specific cation modes can be used as a powerful probe in conjunction with X-ray diffraction and other techniques[11,12] in locating previously unidentified cations. Also we will outline a self-consistent methodology for assigning the far-infrared spectra of metal ion-exchanged faujasite zeolites. Each site will be dealt with separately and the discussion will be illustrated with several key examples obtained from recent advances in our laboratory. We focus attention here on the uni- and divalent metal cations, whilst trivalent rare-earth cations will form the subject of another study.[30]

Experimental Section

Transition-metal ion-exchanged zeolites were prepared from sodium zeolite X (Linde 13×: Si/Al = 1.25) and sodium Y (Linde LZ-Y52: Si/Al = 2.5) which had been slurried with 0.1 M NaCl solution to remove sodium defect sites, washed until free of chloride, and calcined in dry oxygen at 500 °C for 16 h. After rehydration, the zeolite was stored over saturated ammonium chloride to maintain a constant humidity. Ion exchange was affected at room temperature with 0.01 N solutions of the chlorides (Mn, Co, Ni, and Ca) or nitrates (Cu and Zn) according to standard techniques. In a typical experiment between 1 and 2 g of the sodium zeolite was weighed out and slurried with 3 L of the corresponding transition-metal solution. The pH of the resulting mixture was between 6 and 6.5 and was stirred for 20 h. After filtration, the sample was washed until the washings were free of anion (chloride or nitrate) and then dried at 100 °C, lightly ground to a coarse powder, and stored over saturated ammonium chloride. The iron(II) sample was prepared in an analagous fashion from the sulfate by using deoxygenated water and low pH (4–5). After exchange, the sample was handled under anaerobic conditions.

The samples were analyzed by inductively coupled plasma emission spectroscopy (ICP) and in some cases by neutron activation by using the U of T Slow Poke reactor facility. The results of the analyses are presented below.

sample	anal. results	sample	anal. results
NaX	$Na_{86}Y$	$Co_{14}Y$	$Co_{14}Na_{28}Y$
NaY	$Na_{56}Y$	$Co_{17}Y$	$Co_{17}Na_{22}Y$
CaY	$Ca_{21.5}Na_{13.0}Y$	NiY	$Ni_{21.2}Na_{13.6}Y$
MnY	$Mn_{18.3}Na_{19.4}Y$	CuY	$Cu_{13.2}Na_{29.6}Y$
FeY	$Fe_{14.6}Na_{26.8}Y$	ZnY	$Zn_{21.1}Na_{13.8}Y$
Co_6Y	$Co_6'Na_{44}Y$		

To ensure that the integrity of the zeolite lattice was maintained after exchange, the samples were studied by powder X-ray diffraction and

(1) Maxwell, I. E. *Adv. Catal.* **1982**, *31*, 1.
(2) Gallezot, P. *Catal. Rev. Sci. Eng.* **1978**, *17*, 273.
(3) Breck, D. W. "Zeolite Molecular Sieves"; Wiley Interscience: New York, 1974.
(4) Gallezot, P.; Alarcon-Diaz, A.; Dalmon, J.-A.; Renouprez, A. J.; Imelik, B. *J. Catal.* **1975**, *39*, 334.
(5) Beyer, H.; Jacobs, P. A.; Uytterhoeven, J. B. *J. Chem. Soc., Faraday Trans. 1* **1976**, *72*, 674.
(6) Bergeret, G.; Gallezot, P.; Imelik, B. *J. Phys. Chem.* **1981**, *85*, 411.
(7) Gellens, L. R.; Smith, J. V.; Pluth, J. J. *J. Am. Chem. Soc.* **1983**, *105*, 51.
(8) Mortier, W. J. "Compilation of Extra Framework Sites in Zeolites"; Butterworth: Washington, DC, 1982.
(9) Pearce, J. R.; Mortier, W. J.; Uytterhoeven, J. B. *J. Chem. Soc., Faraday Trans. 1* **1979**, *75*, 898.
(10) Ozin, G. A.; Baker, M. D.; Godber, J. *J. Phys. Chem.* **1985**, *89*, 305; **1984**, *88*, 4902. Ozin, G. A.; Baker, M. D.; Godber, J. *J. Phys. Chem.*, in press; *Catal. Rev. Sci. Eng.*, in press.
(11) Narayana, N.; Kevan, L. *J. Chem. Phys.* **1982**, *76*, 3999.
(12) Lai, P. P.; Rees, L. V. C. *J. Chem. Soc., Faraday Trans 1* **1972**, *72*, 1818.

0002-7863/85/1507-3033$01.50/0

Table I. Vibrational Properties of Metal Cations in Sites I, I', II, III', and III'' of Faujasite Zeolites

				
cation site	I	I', II	III'	III''
local site symmetry	O_h	C_{3v}	C_{4v}	C_{s},
asymmetric vibration	T_{1u}	E	E	A'
G-matrix element	$\mu_O + 2\mu_M$	$\mu_O + \mu_M(1 - \cos\alpha')$	$\mu_O + \mu_M(1 - \cos\alpha'')$	$\mu_O + \mu_M(1 - \cos\alpha''')$
F-matrix element	$k_r - k_{rr}$	$k_r - k_{rr}$	$k_r'' - k_{rr}$	$k_r''' - k_r'''$

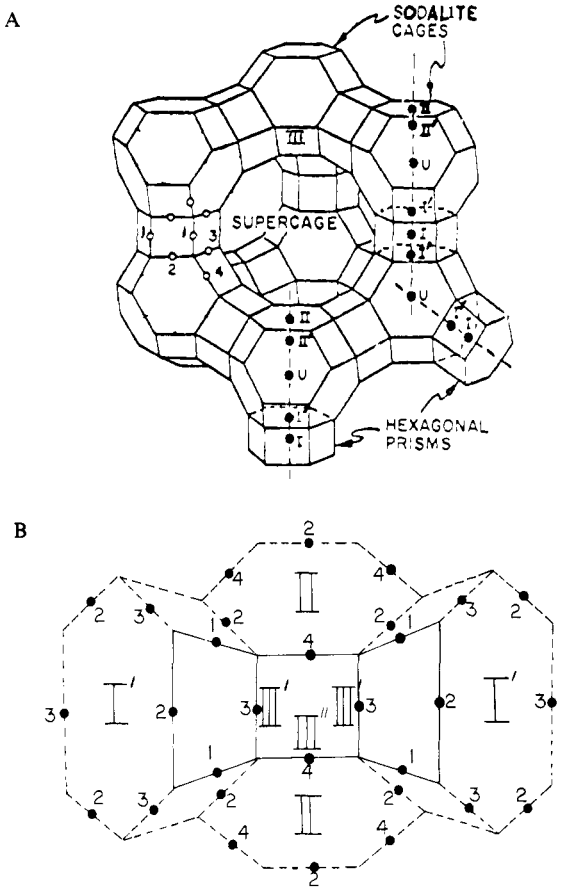

Figure 1. (A) (Top) Perspective view of faujasite zeolite. The four crystallographically distinct framework oxygens are indicated on the figure along with specific cation sites as discussed in the text. (B) (Bottom) Smith's designation of cation and framework oxygen sites in faujasite.

compared to the starting material. No evidence was found for any alteration of the zeolite lattice. The zeolite powder samples were pressed into self-supporting 20 mm diameter wafers weighing approximately 20 mg by using an applied pressure of between 5 and 8 tons per square inch for up to 25 s. The wafers were clamped into the sample holder of an in situ vacuum cell equipped with high density polyethylene windows, which was mounted in the vacuum chamber of a Nicolet 200 SXV FT-Far-IR spectrometer.[10] The sample wafers could be moved within their own vacuum system to intersect the IR beam and to a furnace area where dehydration or reaction chemistry could be performed over the range of 10 to ca. 600 °C. The samples were dehydrated in situ by heating to above 450 °C in vacuo for up to 10 h. The level of dehydration was judged by complementary mid-IR spectroscopy and in most cases was found to be essentially complete. Complications due to incomplete dehydration and the far-IR spectroscopy of partially hydrated zeolites will be the topic of further studies. The spectra were recorded by using a globar source, TGS detector and 6.25-μm Mylar beam splitter. The spectra reported are the result of the coaddition of 500 interferograms encompassing 30-min collection time, although survey spectra of a useable quality could be obtained in less than a minute. The spectral resolution in all cases is 4 cm^{-1}, and most of the spectra have been base line corrected.

Curve analysis was performed with the Nicolet interactive software package in the manual mode. The curve analyses shown in this paper were affected by fitting the observed vibrational spectra to 100% Gaussian lines. A number of well-founded criteria were used in the curve resolution procedure, in order to obtain a consistent match between the observed and simulated spectra. The number of Gaussian lines used was kept to a minimum, bearing in mind how many cation site vibrations were expected (i.e., I, I', II, and III). The bands denoted by asterisks in Figures 7–12, which are probably due to symmetric metal cation vibrations (as discussed in the text), arose naturally from the computer simulation. It is important to note that the area of these bands is sufficiently small that their presence in the simulated spectra does not alter the overall trends and conclusions of the intensity analysis.

Frequencies of Metal Cation Far-IR Vibrations in Faujasite Zeolites

One of the primary aids used for assigning site-specific far-IR metal cation absorption spectra stems from a seminal contribution of Brodskii et al.[14,15] who proposed a simple relationship between the cation vibrational frequency ν_i for a particular lattice site i, and the mass M_i and ionic radius R_i of the cation residing in that site. Although not directly stated in the literature, this expression appears to derive from the combined use of the diatomic harmonic oscillator approximation for a symmetric vibration of an n-coordinate $M^{q+}O_n$ site, where the cation M^{q+} is assumed to vibrate against a rigid framework (infinite lattice mass), in conjunction with the harmonic M–O bond stretching force constant k_r. Although there are a number of ways of empirically describing force constant dependence on bond length, the most familiar being Clark's,[16] Allen and Longair's,[17] Gordy's,[18] and Badger's[19] rules, it is the latter inverse cube rule that appears to be most generally applicable to polyatomic systems and is the one favored by Brodskii et al.[14,15] in his work with metal zeolites, namely, $\nu_i = C_B M_i^{-1/2} R_i^{-3/2}$ where C_B will be referred to as the Brodskii constant. The applicability and usefulness of this simple relationship was originally established for alkali-metal ion-exchanged faujasites.[13-15] However, its extension in our laboratory to the assignment of the far-IR cation modes in a range of transition-metal ion-exchanged faujasites has raised some interesting new problems which necessitate a reexamination of the model used to derive the Brodskii expression.

Some of the immediate questions and more obvious anomalies that arise from our transition-metal M^{2+} faujasite work[10,25,26] and that require attention include (a) the cation site frequency order II > I > III > I' compared to II > I > I' > III in alkali-M^+ faujasites, (b) the anomalously high frequencies of all of the transition-metal 2+ cation site modes compared to the respective alkali-metal 1+ modes; and (c) and the special properties of site III cation modes, where the locations of sites I, I', II, and III are schematically represented in Figure 1.

Before expanding upon each of these points (as well as others), we will first set up secular equations for the various cation sites of faujasite for the purpose of calculating their respective vibrational frequencies. A first approximation to this problem (to make

(13) Peuker, C.; Kunath, D. *J. Chem. Soc., Faraday Trans 1* **1981**, *77*, 2079.
(14) Brodskii, I. A.; Zhdanov, S. P. *Proc. Int. Conf. Zeolites, 5th* **1980**, 234–241.
(15) Brodskii, I. A.; Zhdanov, S. P.; Stanevic, A. E. *Opt. Spectrosc.* **1971**, *30*, 58.
(16) Clark, C. H. Douglas *Philos. Mag.* **1934**, *18*, 459.
(17) Allen, H. S.; Longair, A. K. *Nature (London)* **1935**, *135*, 764.
(18) Gordy, W. *J. Chem. Phys.* **1946**, *14*, 305.
(19) Badger, R. M. *J. Chem. Phys.* **1934**, *2*, 128; **1935**, *3*, 710.

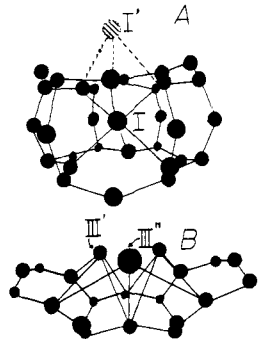

Figure 2. Perspective view of (A) the site I and I' M^{2+} cations in the hexagonal prism and adjacent to a six ring in the β-cage and (B) the site III' and III'' M^{2+} cations at the sequence of four rings in dehydrated $M^{2+}ZY$. (N.B. sites III' and III'' are never simultaneously occupied).

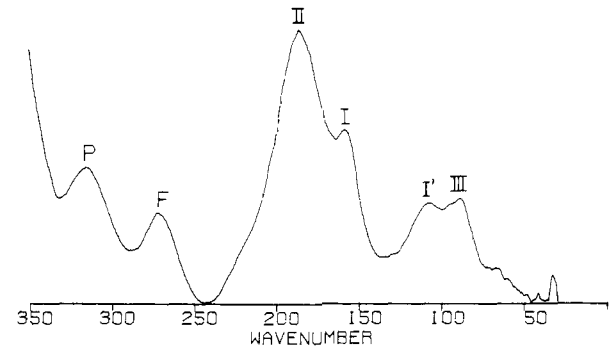

Figure 3. Far-IR absorbance spectrum (350–30 cm^{-1}) of vacuum thermally dehydrated $Na_{56}Y$ (Si/Al = 2.5). The site assignments discussed in the text are shown on the bands. (P denotes a pore opening mode and F an oxygen framework vibration).

it analytically tractable) involves the use of a local molecule approximation for each $M^{q+}O_n$ cation site, decoupling out deformational modes (actually high-frequency framework oxygen vibrations), and determination of the appropriate symmetrized **G** and **F** matrix elements. These are listed in Table I for the most intense (see later) asymmetric stretching modes of metal cations in sites I, I', II, III', and III''.

A few points about the structures of cations in sites III' and III'' are in order here. These cations reside over the sequence of four rings in the large cavity as illustrated in Figure 2. The local symmetry of both of these sites is C_s although for vibrational purposes site III' can be considered to have pseudo-C_{4v} symmetry. From a vibrational point of view, site III' in C_{4v} symmetry has $A_1 + B_1 + E$ $\nu(MO_4)$ cation modes of which the $A_1 + E$ are IR active with the asymmetric E mode expected to have the greater IR intensity (see later). Site III'' cations in C_s symmetry have $2A' + A''$ $\nu(MO_3)$ cation modes, of which the asymmetric A'' is likely to be the most intense, with some slight IR activity from at least one of the A' modes (see later).

The **G**- and **F**-matrix elements in Table I are each used in the vibrational secular equation

$$\mathbf{GF} - \lambda = 0$$

where $\lambda = 4\pi^2c^2\nu^2/N$ and ν is in inverse centimeters when **G** is expressed in atomic mass units. When the bond stretching force constants are expressed in units of millidynes per angstrom then

$$\lambda = 0.58885(\nu/1000)^2 = A\nu^2$$

Recall that the Badger rule in its full form is written

$$k_r = C/(r_e - d)^3$$

Here the bond stretching force constant k_r (neglecting the stretch–stretch interaction term) is related to the inverse cube of the equilibrium internuclear distance r_e of the respective bond, where C and d are kept constant through a group of similar molecules but can vary from group to group in the periodic chart. We will refer to C as the Badger constant. (In the work of Batsanov and Derbeneva,[20] we note that the bond stretching force constants are scaled as proportional to $1/r_e^3$.) We can therefore write for each IR-active cation site asymmetric ν_{M-O} mode the following secular equations:

site I $\quad \nu^2 = [C/A(r - d)^3](\mu_O + 2\mu_M)$

site I' $\quad \nu^2 = [C'/A(r' - d')^3](\mu_O + \mu_M[1 - \cos \alpha'])$

site II $\quad \nu^2 = [C'/A(r' - d')^3](\mu_O + \mu_M[1 - \cos \alpha'])$

site III' $\quad \nu^2 = [C''/A(r'' - d'')^3](\mu_O + \mu_M[1 - \cos \alpha''])$

site III'' $\quad \nu^2 = [C'''/A(r''' - d''')^3](\mu_O + \mu_M[1 - \cos \alpha'''])$

(20) Batsanov, S. S.; Derbeneva, S. S. *Zh. Strukt. Khim.* **1969**, *10*, 602.

At this stage we have kept the model as general as possible by retaining the nonprimed and primed notation for C, r, d, and α to signify bond length, angle, and coordination number differences at each cation site. Thus, to obtain the Brodskii relationship for cation site vibrational frequencies, $\nu = C_B M^{-1/2} R^{-3/2}$, it is clear that for each site, $r - d$ is equated with the cation ionic radius R, and the reciprocal mass of the nearest-neighbor oxygen ions μ_O is put equal to zero; this is equivalent to a rigid framework (infinite lattice mass) approximation. Thus, we obtain

site I $\quad \nu = (C/A)^{1/2}[R^{-3/2}M^{-1/2}(2)^{1/2}]$

site I' $\quad \nu = (C'/A)^{1/2}[R^{-3/2}M^{-1/2}(1 - \cos \alpha')^{1/2}]$

site II $\quad \nu = (C'/A)^{1/2}[R^{-3/2}M^{-1/2}(1 - \cos \alpha')^{1/2}]$

site III' $\quad \nu = (C''/A)^{1/2}[R^{-3/2}M^{-1/2}(1 - \cos \alpha'')^{1/2}]$

site III'' $\quad \nu = (C'''/A)^{1/2}[R^{-3/2}M^{-1/2}(1 - \cos \alpha''')^{1/2}]$

One discovers therefore that the original Brodskii equation in essence considers only a single metal cation vibrational mode and makes no attempt to allow for structural changes at a cation lattice site, which in the above frequency expressions originates from the **G**-matrix elements and involves O–M̂–O bond angle terms, which are different for each cation site. Thus, the Brodskii constant C_B for a particular cation site can be identified with the Badger constant and its accompanying **G**-matrix angular function.

In terms of the vibrational frequency of identical cations residing in sites I, I', and III, one might intuitively expect the three coordinate site I' cation to have the highest frequency with the six coordinate site I lowest. In the case of alkali-ion-exchanged faujasites, there has, however, been some disagreement on this assignment,[13,14] although most authors prefer to ascribe the higher frequency band to site I cations as indicated in Figure 3, which shows the far-IR spectrum of vacuum thermally dehydrated $Na_{56}Y$. The site assignments are indicated in Roman numerals in standard nomenclature according to Figure 1. We believe this assignment is correct on the grounds that the predicted frequency ratio of 1.85:1.31:1.00 for Na^+ cations in sites I, I', and III (see later) determined from the above expressions by using X-ray crystallographic α values of 90°, 90°, and 65.6° respectively, and assuming identical Badger constants C_B, compare favorably with the observed frequency ratio of 1.81:1.23:1.00 obtained from Figure 3.

In this context, we note that the alkaline-earth 2+ and transition-metal 2+ ion-exchanged faujasites appear to show different behavior with an anomalously high cation site III'' vibration and a frequency order of I > III'' > I'. Support for this assignment can again be found from use of the above secular equations which for Ca^{2+} through to Zn^{2+} anticipate a frequency ratio of around 1.41:1.33:1.00 for M^{2+} cations in sites I, III'' (see later), and I' by using representative α values of 90°, 90°, and 140°, respec-

Table II. Calculated and Observed Metal Cation Far-IR Vibrational Frequencies for Sites I, I′, II, and III in $M^{2+}Y$ Faujasites

	cation site	Ca^{2+}	Mn^{2+}	Fe^{2+}	Co^{2+}	Ni^{2+}	Cu^{2+}	Zn^{2+}
I	obsd	130.6	160.7	165	170	176.5	163	162
	calcd (Na^+)	122.9	135.8	146	148.6	160.4	146.5	140.6
	calcd(Ni^{2+})	135.1	149.3	160.5	165.7	176.5	160.7	157.1
	$\nu_{M^{2+}}(Ni^{2+})/\nu_{M^{2+}}(Na^+)$	1.09	1.09	1.09	1.09	1.10	1.09	1.11
I′	obsd	91.2	101	105	104	116.3	106	103
	calcd(Na^+)	83.2	91.9	97.4	100.6	108.6	99.2	95.2
	calcd(Ni^{2+})	88.8	99.1	105.6	109.4	116.3	106.2	103.5
	$\nu_{M^{2+}}(Ni^{2+})/\nu_{M^{2+}}(Na^+)$	1.06	1.07	1.07	1.07	1.07	1.07	1.08
II	obsd							
	calcd(Na^+)	144.6	159.8	169.4	175.0	188.8	172.5	165.5
	calcd(Ni^{2+})	160.9	177.6	191.2	197.6	210.0	191.8	186.9
	$\nu_{M^{2+}}(Ni^{2+})/\nu_{M^{2+}}(Na^+)$	1.11	1.11	1.11	1.11	1.11	1.11	1.11
III	obsd		140.2	139.2	142	148.1	137	126
	calcd(Na^+)	69.3	76.6	82.4	85.2	90.7	82.7	80.5
	calcd(Ni^{2+})	113.0	126.6	134.8	139.2	148.1	135.3	131.8
	$\nu_{M^{2+}}(Ni^{2+})/\nu_{M^{2+}}(Na^+)$	1.63	1.65	1.63	1.63	1.63	1.63	1.63

tively. The observed frequency ratios shown below are in remarkably close agreement with the predicted values

	I:III″:I′
Ca^{2+}	1.432:–:1
Mn^{2+}	1.591:1.388:1
Fe^{2+}	1.650:1.395:1
Co^{2+}	1.635:1.365:1
Ni^{2+}	1.547:1.273:1
Cu^{2+}	1.583:–:1
Zn^{2+}	1.573:1.223:1

thereby lending credance to the M^{2+} cation site frequency assignments.

Another interesting point in this same vein relates to the use of the original Brodskii expression for estimating the Ca^{2+} to Zn^{2+} frequencies based on Na^+ and Ni^{2+} reference cation frequencies for sites I, I′, II, and III assuming initially that the ratios of the respective Brodskii constants $C_{M^{2+}}(Na^+)/C_{Na^+}(Na^+)$ and $C_{M^{2+}}(Ni^{2+})/C_{Ni^{2+}}(Ni^{2+})$ are both equal to unity. One discovers from this series of calculations that the Ca^{2+} to Zn^{2+} frequencies are reproduced quite well using the Ni^{2+} frequency basis set, whereas they are all too low when the respective Na^+ values are utilized, as judged from Table II.

What is particularly striking from this set of data is the remarkably constant frequency ratio $\nu_{M^{2+}}(Ni^{2+})/\nu_{M^{2+}}(Na^+)$ for $M^{2+}Y$ derived from the Ni^{2+} and Na^+ basis sets, respectively, namely about 1.09 for M^{2+} cations in sites I, I′, and II as seen in Table II. If one examines analytically the origin of these ratios for M^{2+} in a particular cation site, one obtains:

Na^+ basis set:

$$\nu_{M^{2+}}(Na^+)/\nu_{Na^+}(Na^+) = \frac{C_{M^{2+}}(Na^+)}{C_{Na^+}(Na^+)}\left(\frac{M_{Na^+}{}^{1/2}R_{Na^+}{}^{3/2}}{M_{M^{2+}}{}^{1/2}R_{M^{2+}}{}^{3/2}}\right)$$

Ni^{2+} basis set:

$$\nu_{M^{2+}}(Ni^{2+})/\nu_{Ni^{2+}}(Ni^{2+}) = \frac{C_{M^{2+}}(Ni^{2+})}{C_{Ni^{2+}}(Ni^{2+})}\left(\frac{M_{Ni^{2+}}{}^{1/2}R_{Ni^{2+}}{}^{3/2}}{M_{M^{2+}}{}^{1/2}R_{M^{2+}}{}^{3/2}}\right)$$

which yields

$$\nu_{M^{2+}}(Ni^{2+})/\nu_{M^{2+}}(Na^+) = C_{M^{2+}}(Ni^{2+})/C_{M^{2+}}(Na^+)$$

These are the frequency ratios listed in Table II for each M^{2+} cation in its various sites. On comparing this frequency ratio with the corresponding one derived from our secular equations for a specific cation site mode, one finds in addition to a ratio of Badger constants, an angular function of the form $[(1 - \cos \alpha_{Ni^{2+}})/(1 - \cos \alpha_{Na^+})]^{1/2}$. This implies that in the case of M^{2+} cations in sites I, I′, and II, the frequency ratio of 1.09 might be traceable to small, essentially constant, differences in α on passing from Na^+ to M^{2+} sites rather than to alterations in the Badger constants. Thus, on altering α from approximately 85° to 95° in the secular equation angular functions, one obtains a ratio of 1.19. One way to understand the much larger frequency ratio for site III cations in Table II without involving changes in the Badger constant on passing from Na^+ is to propose that for Na^+, it is mainly site III′ that is populated (α = 65.6°) whereas for M^{2+} it is instead mainly site III″ (α = 140°). This yields a calculated frequency ratio $\nu_{M^{2+}}(Ni^{2+})/\nu_{M^{2+}}(Na^+)$ for site III cations of 1.74 which is reasonably close to the value of 1.63 listed in Table II. Note that the occupancy of site III″ by transition metals has no crystallographic basis and therefore the proposed residence of metal cations in this site is not necessarily valid. Nonetheless the O–$\hat{M}$–O angle of ~140° for site III″ has been used in this paper and seems to predict well the measured spectra both in the frequency and intensity analysis, whereas an angle of ~65° (site III′) does not.

A similar trend in the frequency ratios was observed by using $Ni^{2+}X$ (Si/Al = 1.25) and Na^+X as references. The values for the frequency ratios in this case were essentially the same as those determined with the Y-type zeolites. An important conclusion from these data is that the product of the Badger constant and the angular function, $(1 - \cos \alpha)^{1/2}$, remains invariant to changes in the Si/Al ratio. If we assume, as did Badger, that his constant C_B will remain unaffected in groups of similar molecules, we must then also deduce that the O–$\hat{M}$–O angles for a particular M^{2+} cation do not differ appreciably in X and Y ion-exchanged zeolites.

As an aside, it is necessary to explain the method used for obtaining the α values used for Na^+ and M^{2+} in sites III′ and III″, respectively. Our approach was based on X-ray crystallographic data for vacuum thermally dehydrated and oxidized Ag^+ faujasite X.[21] This choice was dictated by the fact that the heavy mass of silver makes it possible to locate virtually all the Ag^+ ions in this faujasite structure including those at sites III′ and III″, as illustrated in Figure 2. Unfortunately this is not the state of affairs for Na^+ and most first transition series M^{2+} faujasites so the required experimental α values are not accessible.[8] From this structure and those of Na^+Y[22] and $Ni^{2+}Y$,[23] one can obtain the respective site I′ metal–oxygen bond lengths, namely $Ag^+(I')$–$3O_3$ = 2.67 Å, $Na^+(I')$–$3O_3$ = 2.30 Å, and $Ni^2(I')$–$3O_3$ = 2.15 Å. With these numbers, "bond length reduction factors" relating Ag^+ to Na^+ and Ag^+ to Ni^{2+} faujasite are calculated to be 0.865 and 0.808, respectively. These values are then applied to the Ag^+(III′)–$2O_1$, Ag^+(III′)–$2O_4$ and Ag^+(III″)–$2O_1$, Ag^+(III″)–O_4 bond lengths to obtain the respective values for Na^+(III′) and Ni^{2+}(III″). These are then used to evaluate $Na^+(\alpha')$ and $Ni^{2+}(\alpha'')$ for sites III′ and III″, respectively. With these α values, one computes $[(1 - \cos \alpha'')/(1 - \cos \alpha')]^{1/2}$ to yield the desired frequency ratio $\nu_{M^{2+}}(Ni^{2+})/\nu_{M^{2+}}(Na^+)$.

Up to now we have neglected to comment on the surprisingly high frequency assigned to cation site II modes. Based on our

(21) Gellens, L. R.; Mortier, W. J.; Uytterhoeven, J. B. *Zeolites* **1981**, *1*, 11.

(22) Eulenberger, G. R.; Shoemaker, D. P.; Keil, J. G. *J. Phys. Chem.* **1967**, *71*, 1812.

(23) Gallezot, P.; Imelik, B. *J. Phys. Chem.* **1973**, *77*, 652.

secular equations and approximations for a three-coordinate $M^{q+}O_3$ lattice site, it would have been anticipated to fall in the region of site I′ modes; this does not accord well with the deductions from those experiments specifically designed to test this assignment (see later). Although changes in C, R, α, and $k_r - k_{rr}$ can all be invoked to explain the frequency of site II relative to those of sites I, I′, and III, it is tenuous at best with the available data to try to pin down the contribution of each term to the observed effect. In this context, other questions that remain concern the validity of the quasimolecule and infinite lattice site $\mu_O = 0$ approximations, decoupling out deformational modes, constancy of the Badger constant on passing from one long period to the next (or even one element to its neighbor) and on changing cation oxidation states, substitution of the Badger $(r - d)$ term for the metal cation ionic radius R, and the neglect of stretch–stretch interaction force constants $k_{rr'}$. In the sections that follow, we will discuss each cation site vibrational mode for some key alkali, alkaline-earth, and transition-metal ion-exchanged faujasites and then move to the subject of the intensities of far-IR cation vibrational modes.

(A) Sites I and I′. The locations of sites I and I′ are schematically represented in Figure 1. Site I is situated at the center of the hexagonal prism, and ions at this site are octahedrally coordinated to six O_3-type framework oxygens. Site I′ is located within the sodalite cage near the six-ring between the hexagonal prism and the sodalite cage. Cations residing at this position are threefold-coordinated (C_{3v} symmetry) to oxygens of the sodalite six-rings. Since cations in this site share three O_3 oxygens of the bridging hexagonal prism, it is unlikely from electrostatic considerations that sites I and I′ are simultaneously occupied.

Credance for the assignment of site I cation modes at higher frequencies than site I′, as discussed earlier, can be found in the far-IR spectra data for $Ca_{21.5}Na_{13}Y$ to be described. The X-ray crystallography of calcium ion-exchanged faujasite $Ca_{27}Y$[8] shows that the major calcium site occupancies are in sites I, I′, and II. The exact occupancy factors are

	I	I′	II	unlocated
$Ca_{27}Y$	14.2	2.6	11.4	0

Using the assignments of Figure 3 and the secular equations for sites I and I′, we can predict the vibrational frequencies of calcium ions in these sites (Ca^{2+}; R = 1.14 Å; M = 40.08). These are

	I	I′	II
calcd	135.1	88.8	160.9
obsd	130.6	91.2	200.0

On the basis of this model, the assignments shown in Figure 3, and the X-ray data for Ca_{27} Y, one would therefore predict that the major far-IR band in the calcium faujasite spectrum would appear near 135 cm^{-1}. The far-IR spectrum of $Ca_{27}Y$ is shown in Figure 4. Clearly the agreement between the observed and predicted frequencies is extremely good. The data strongly indicate that site I M^{2+} cation vibrations occur at higher frequencies than site I′. Intensity arguments presented later strongly support this proposal.

(B) Site II. The identification of cation vibrations associated with site II occupancy is quite clear-cut. Site II cations are situated within the supercage adjacent to the six-rings of the sodalite cages having C_{3v} site symmetry. Since this cation is directly affected by molecules present in the supercage, it is easily discernible from the behavior of its far-IR absorption which is seen, for example, to red shift upon pyridine adsorption.[24] Further credance for the assignment of the band at 186 cm^{-1} to site II Na^+ ions comes from recent work in our laboratory[25] on a series of transition-metal 2+ ion-exchanged faujasites, shown in Figure 5. When a sodium Y zeolite is ion-exchanged to produce $M^{2+}ZY$, the residual sodium ions occupy site II. The absorption band due to residual sodium is clearly visible and is indicated by a capital S in Figure 5. Again

(24) Butler, W. M.; Angell, C. L.; McAllister, W.; Risen, W. M. *J. Phys. Chem.* **1977**, *81*, 2061.
(25) Ozin, G. A.; Baker, M. D.; Godber, J. *J. Am. Chem. Soc.* in press.

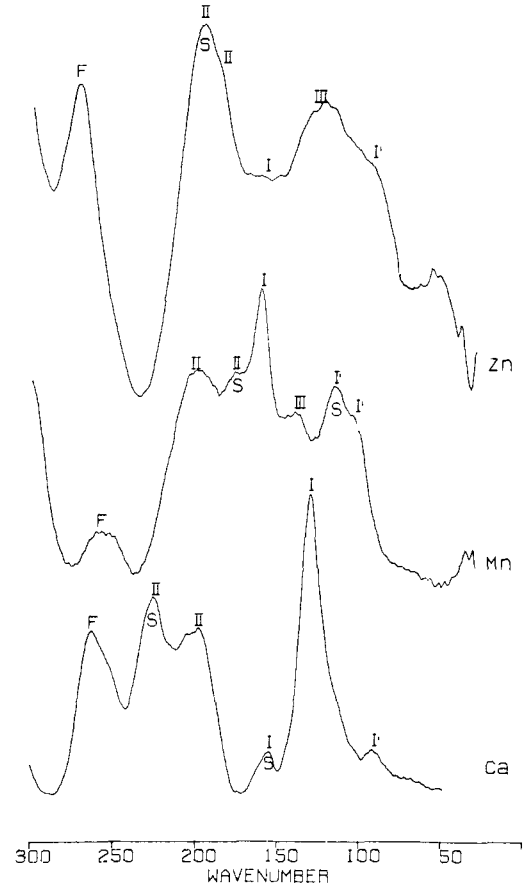

Figure 4. Far-IR absorbance spectrum of 450 °C vacuum thermally dehydrated $Ca_{21.5}Y$, $Mn_{18.3}Y$, and $Zn_{21.1}Y$. Bands marked with an S denote residual sodium cation vibrations.

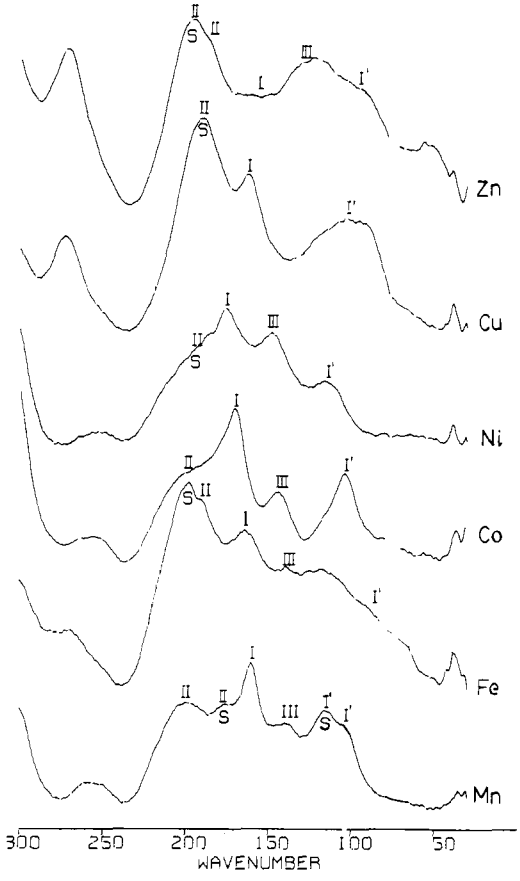

Figure 5. Far IR absorbance spectra of 450 °C vacuum thermally dehydrated Mn^{2+}, Fe^{2+}, Co^{2+}, Ni^{2+}, Cu^{2+} and Zn^{2+} zeolite Y.

intensity analyses described later support this view. It is noteworthy that the site II sodium ion absorption band shifts as its coexisting transition-metal ion is changed. These small shifts can be rationalized in terms of electrostatic considerations whereby the strength of the interaction of the sodium ion with the zeolite framework is dependent upon the local electron density, which is affected by the specific site populations and type of cations throughout the zeolite. It will also become evident in subsequent sections of this paper that frequency shifts can also be caused by angular effects. For example, the frequency of a cation located on a six-ring site II will vary depending on whether the ion projects into the α or β cages. In this way, it is possible, therefore, to distinguish with angular information between cations, for example, in sites II′ and I′.

(C) Site III. Site III cations are located on the walls of the supercage residing at the sequence of four-rings (Figure 2). This site is usually postulated as a possible location for excess cations that are not accommodated at the six-ring sites. However, the large multiplicity of possible I, I′, and II cation sites and the large temperature factors on cations in site III′ and III″, especially for the first-row transition metals, often causes uncertainties in the structural assignment of site III cations by Fourier X-ray techniques. In view of the fact that this site has often been associated with catalytic activity,[1] its identification is of prime importance. Using the secular equation and the frequency of 89.2 cm^{-1} for site III Na^+ ions in sodium Y faujasite we would predict that site III Co^{2+}, for example, would occur at 85.2 cm^{-1}. As described earlier, we have discovered that site III transition-metal 2+ ions give rise to absorption bands at anomalously high frequencies compared to site III alkali-metal ions. This was rationalized in terms of site III″ occupancy for M^{2+} and site III′ for M^+ cations. The bands due to site III transition-metal 2+ cations arise near 150 cm^{-1}, and in the following discussion we will present compelling evidence for this assignment.

As in the case of site II cations, site III″ is directly accessible to supercage adsorbates, and we have previously shown[26] for cobalt ion-exchanged faujasites that the band at 147 cm^{-1} is affected by pyridine adsorption. However, possible adsorbate-induced migrations from sites I and I′ and charge delocalization effects in the zeolite framework make the unequivocal assignment of this band from this data to supercage cobalt 2+ ions somewhat tenuous. Similar bands in this spectral region for MnY, FeY, NiY, and ZnY have been assigned to site III cations.[25] We note that although the X-ray data for CuY samples similar to those used in this study[27] report that site III″ is unoccupied, there is however measurable intensity in the far-infrared spectrum shown in Figure 5 between the site I and I′ modes, signaling the occupancy of site III″ by some copper (2+) cations.

The knowledge that this mode is due to a supercage cation can be used to further expound upon the X-ray analyses of $M^{2+}Y$ zeolites. In what follows we have chosen two examples to illustrate this point. X-ray analyses of $Mn_{19.3}Y$[9] locate manganese ions in sites I(4.6), I′(2.8), and II(10.8). Inspection of the far-IR spectrum of $Mn^{2+}ZY$ in Figure 5 shows that this analysis is probably incomplete since the spectrum shows absorptions due to at least four differently sited manganese cations, where that at 140.2 cm^{-1} is due to site III″ Mn^{2+} ions.

A second example of how far-IR spectroscopy can assist in assigning X-ray data is illustrated by the spectra of cobalt 2+ ion-exchanged faujasite. The X-ray analyses of $Co_{14}Na_{25}Y$ locate an average of 13.5 Co^{2+} ions per unit cell, in sites I and I′[28] although the far-IR spectrum of this sample, shown in Figure 6, indicates quite clearly that site III″ is occupied by cobalt 2+ ions. In higher concentration Co^{2+} ion-exchanged faujasites, the X-ray analyses have not yet been successful in locating the additional cobalt 2+ ions. However, the far-IR spectrum of $Co_{17}Na_{22}Y$

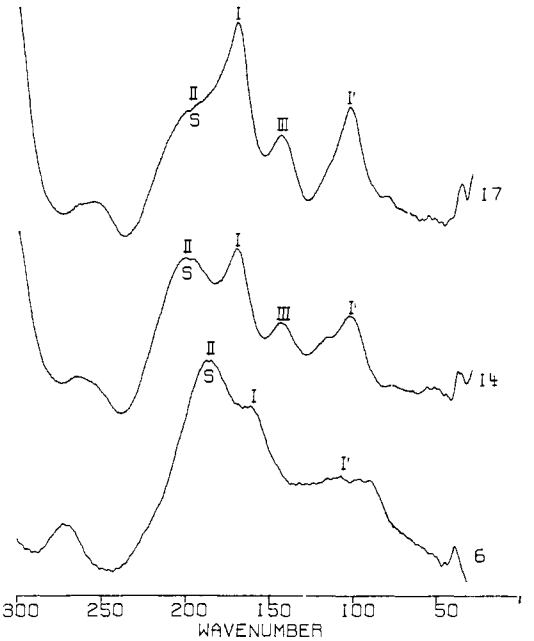

Figure 6. Far IR absorbance spectrum of 450 °C vacuum thermally dehydrated Co_6Y, $Co_{14}Y$, and $Co_{17}Y$.

shown in Figure 6 again clearly shows that they reside in site III″.

Intensities of Metal Cation Far-IR Vibrations in Faujasite Zeolites

In this section we wish to inquire into the possibility of utilizing the measured and calculated integrated intensities of the far-IR absorptions of metal cation vibrational modes, in faujasites, for the purpose of securing metal cation vibrational assignments and specifying cation site occupancies. If successful, this approach would provide valuable information complimentary to that obtainable through **GF**-matrix-type frequency calculations, thereby tightening up on any subsequent deductions which are dependent on a sound knowledge of cation site locations and occupation numbers in the zeolite lattice.

Our approach to this problem utilizes the bond dipole approximation, applied to a model localized $M^{q+}O_n$ n-coordinate site (quasimolecule). This is used to compute analytical expressions for the intensity of the far-IR cation vibrations in different sites. By describing the relevant modes in terms of their symmetry coordinates, the integrated intensity over all coordinates for vibrational modes of a given symmetry type, that couple, can be evaluated from the expression[29]

$$\sum_k I_k = \sum_{k'k''} \left(\frac{\partial \vec{\mu}}{\partial S_{k'}} \right) \left(\frac{\partial \vec{\mu}}{\partial S_{k''}} \right) G_{k'k''}$$

where $\vec{\mu}$ is the transition bond dipole moment and should not be confused with a reciprocal mass defined as μ. If one assumes that the deformational modes of the $M^{q+}O_n$ quasimolecule (that is, the high-frequency oxygen framework vibrations) can be decoupled from the respective metal cation modes of interest (as used in the **GF** frequency calculations), then the problem reduces to one involving the simple comparison of the integrated far-IR intensities of analogous asymmetric ν_{M-O} stretching modes, which in the case of O_h site I, $M^{q+}O_6$, and C_{3v} site I′, $M^{q+}O_3$, quasimolecules amounts to consideration of a single T_{1u} and E cation modes, respectively.

It is then of interest to compare the calculated intensity ratios of far-IR bands assigned to, for example, metal cations in sites I and I′ with their respective occupation numbers deduced from available X-ray crystallographic studies. The results of such a comparison, for a number of well-defined samples, will then enable

(26) Ozin, G. A.; Baker, M. D.; Godber, J. In "Heterogeneous Catalysis"; Lunsford, J. H., Shapiro, B., Eds.; Texas A & M University Press: College Station 1984.
(27) Gallezot, P.; Taarit, Y. B.; Imelik. B. *C. R. Hebd. Seances Acad. Sci., Ser. C* **1971**, *272*, 261.
(28) Gallezot, P.; Imelik, B. *J. Chim. Phys.* **1974**, *71*, 155.
(29) Wilson, E. B.; Decius, J. C.; Cross, P. C. In "Molecular Vibrations"; McGraw-Hill: New York, 1955.
(30) Olken, M.; Ozin, G. A., manuscript in preparation.

one to decide whether or not there is a straightforward connection between the far-IR intensities of metal cation modes and their respective site occupancies. If the answer to this question is affirmative, then the intensity method can be considered to be a useful adjunct to the **GF** frequency approach for assigning metal cation far-IR absorptions in zeolites but with the added advantage that one also has an opportunity to independently establish the numbers and locations of exchangeable metal cations and even angles around the cation.

In this spirit, consider the models of site I and I′ cations shown below.

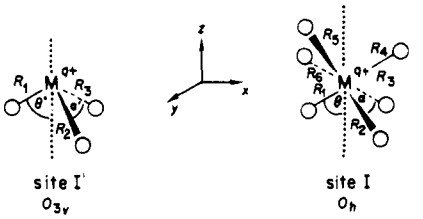

The symmetry coordinates for one component of the degenerate E and T_{1u} asymmetric M–O stretching modes for each site are, respectively, given by

site I′ $$S_E = (1/2)^{1/2}(\Delta R_2 - \Delta R_3)$$

site I $$S_{T_{1u}} = (1/2)^{1/2}(\Delta R_2 - \Delta R_5)$$

where ΔR_i represent the bond stretching internal coordinate for the ith M–O bond. Their application to these $M^{q+}O_n$ systems simply involves the determination of the components of the transition bond dipole moment vectors with respect to each symmetry coordinate, as well as the respective symmetrized $G_{k'k''}$ matrix element

	$\left(\frac{\partial \bar{u}_y}{\partial S_k}\right)$	$G_{k'k''}$
site I; T_{1u}	$(3/2)^{1/2} \sin \theta$	$\mu_O + 2\mu_M$
site I′; E	$(3/2)^{1/2} \sin \theta'$	$\mu_O + \mu_M(1 - \cos \alpha')$

where θ, θ' and α, α' signify that the detailed geometry of sites I and I′ respectively, are not necessarily identical. μ_M and μ_O refer to the reciprocal masses of the metal and oxygen. Remembering the 3:2 weighting of the IR intensities originating from the triple and double degeneracies of the T_{1u} and E modes, one arrives at the intensity expression for cation site I and I′ modes for identical cations as follows

$$\frac{I(\mathrm{SI})}{I(\mathrm{SI}')} = \frac{3 \sin^2 \theta(\mu_O + 2\mu_M)}{2 \sin^2 \theta'(\mu_O + \mu_M[1 - \cos \alpha'])}$$

Using similar reasoning, one can derive the other cation site intensity ratios:

$$\frac{I(\mathrm{SI})}{I(\mathrm{SII})} = \frac{3 \sin^2 \theta(\mu_O + 2\mu_M)}{2 \sin^2 \theta''(\mu_O + \mu_M[1 - \cos \alpha''])}$$

$$\frac{I(\mathrm{SI}')}{I(\mathrm{SII})} = \frac{\sin^2 \theta'(\mu_O + \mu_M[1 - \cos \alpha'])}{\sin^2 \theta''(\mu_O + \mu_M[1 - \cos \alpha''])}$$

For a selection of metal faujasite samples whose cation occupancy for sites I, I′, and II have been established crystallographically, we have used computer-based curve resolution techniques (Figures 7–12) to determine the respective integrated far-IR absorbances. These are summarized in Table III. Using as a first approximation and condition that $\theta = \theta' = \theta''$ and $\alpha = \alpha' = \alpha'' = 90°$, we calculate the far-IR intensity ratios listed in Table III. The agreement between the calculated and observed intensity ratios for all of the samples studied is reasonable for sites I, I′, and II. The differences that are observed probably arise because of the inexact correspondence between the degree of cation exchange of our samples and those used for the X-ray crystallographic determination and the assumption of identical transition bond dipole moment vectors and angular geometries for each cation

LINE	WIDTH	INTENSITY	UNITS	AREA	%AREA
A	21.86	94	4128.48	363	7.3
B	42.12	132	3896.58	981	19.8
C	11.82	22	3618.19	43	.8
D	19.72	215	3488.85	746	15.1
E	33.77	414	3118.99	2469	49.9
F	23.28	82	2799.62	336	6.8

TOTAL AREA = 19758

RMS ERROR = 3.58

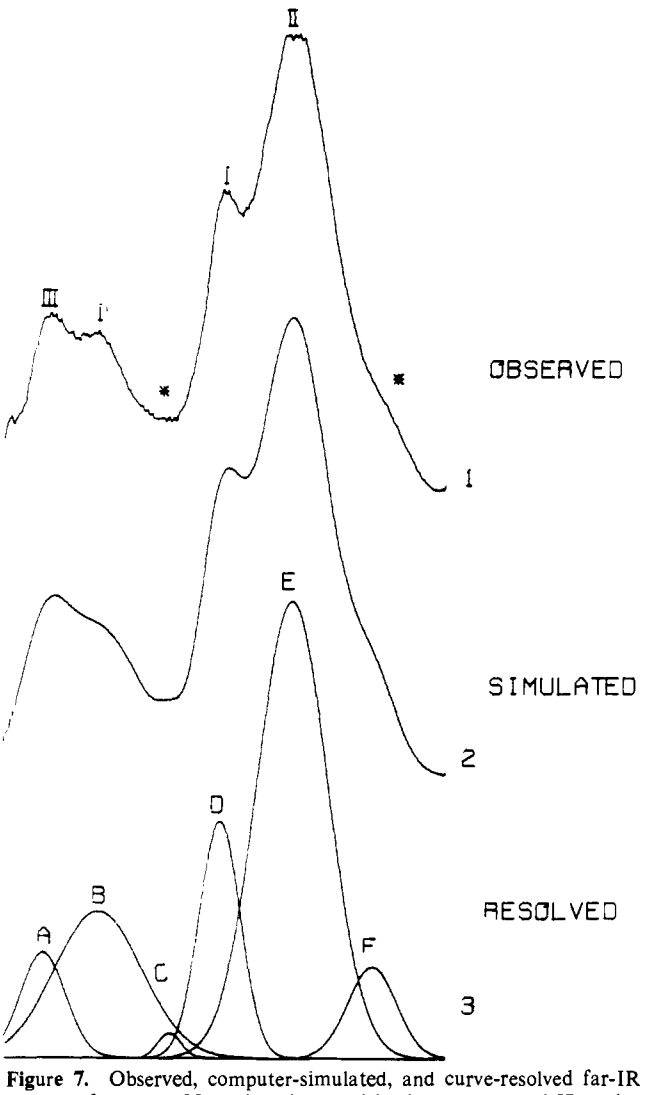

Figure 7. Observed, computer-simulated, and curve-resolved far-IR spectra of $Na_{56}Y$. Note that the asterisks denote proposed IR-active symmetric metal cation vibrations (see text).

lattice site used in the intensity expression. Clearly these are areas where the computations can be further refined in future studies. Nevertheless, at this level of approximation, it is clear that trends in the cation site intensity ratios are reasonably well reproduced by the calculations, and we do not expect refinements of the above type to affect the overall conclusions of this analysis.

A Test Case: Calculation of O–M̂–O Angles in $Ni^{2+}Y$ and $Cu^{2+}Y$

As a further example of the applicability of the theory described in this paper, we will now outline how the O–M̂–O bond angles for sites I, I′, II, and III can be calculated from the vibrational spectrum.

Recall that

$$\nu = C_B/(MR^3)^{1/2}$$

and

$$\nu = (C/(MR^3)^{1/2})(1 - \cos \alpha)^{1/2}$$

thus

$$C_B = C(1 - \cos \alpha)^{1/2}$$

LINE	WIDTH	INTENSITY	UNITS	AREA	%AREA
A	13.92	67	4513.01	79	3.9
B	21.38	123	4337.92	194	10.9
C	23.41	141	4105.14	245	13.8
D	17.29	139	3884.73	179	10.0
E	14.92	32	3689.04	35	2.0
F	26.15	79	3365.62	153	8.6
G	25.31	366	3073.12	689	38.7
H	27.42	184	2809.44	211	11.8

TOTAL AREA = 14231

RMS ERROR = 3.11

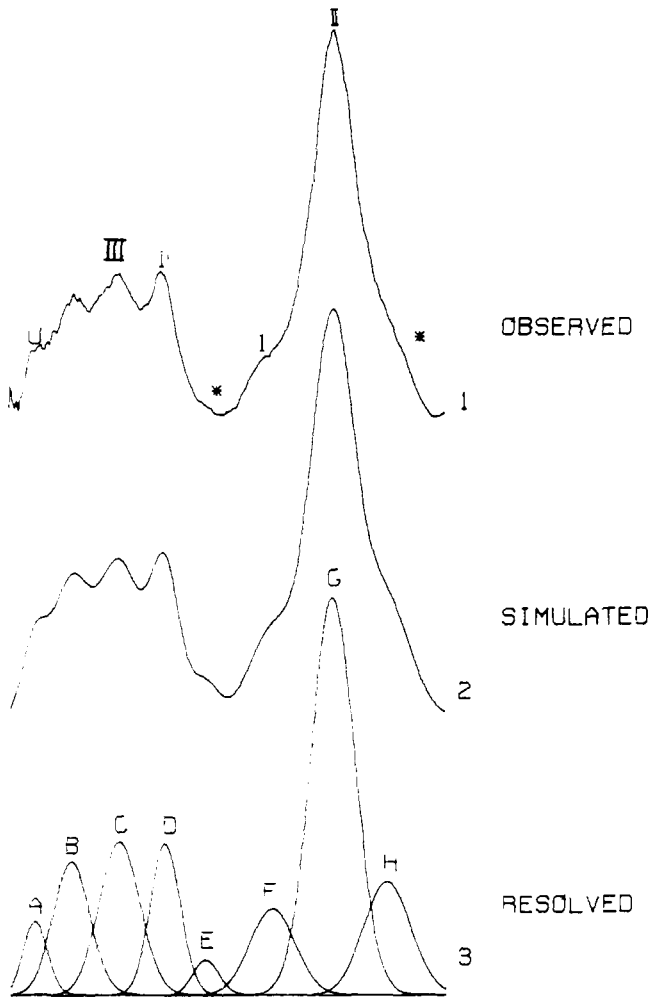

Figure 8. Observed, computer-simulated, and curve-resolved far-IR spectra of $Na_{86}X$. Note that the asterisks denote proposed IR-active symmetric metal cation vibrations (see text).

LINE	WIDTH	INTENSITY	UNITS	AREA	%AREA
A	17.79	31	4192.47	19	2.1
B	12.88	55	4057.29	24	2.5
C	19.99	136	3816.96	92	10.4
D	13.62	346	3671.05	169	18.1
E	11.20	47	3542.38	18	2.0
F	13.48	61	3488.68	29	3.1
G	29.44	216	2965.89	226	24.3
H	19.55	220	2699.82	153	16.4
I	23.73	184	2396.46	155	16.7
J	10.98	92	2282.83	36	3.8

TOTAL AREA = 14885

RMS ERROR = 4.49

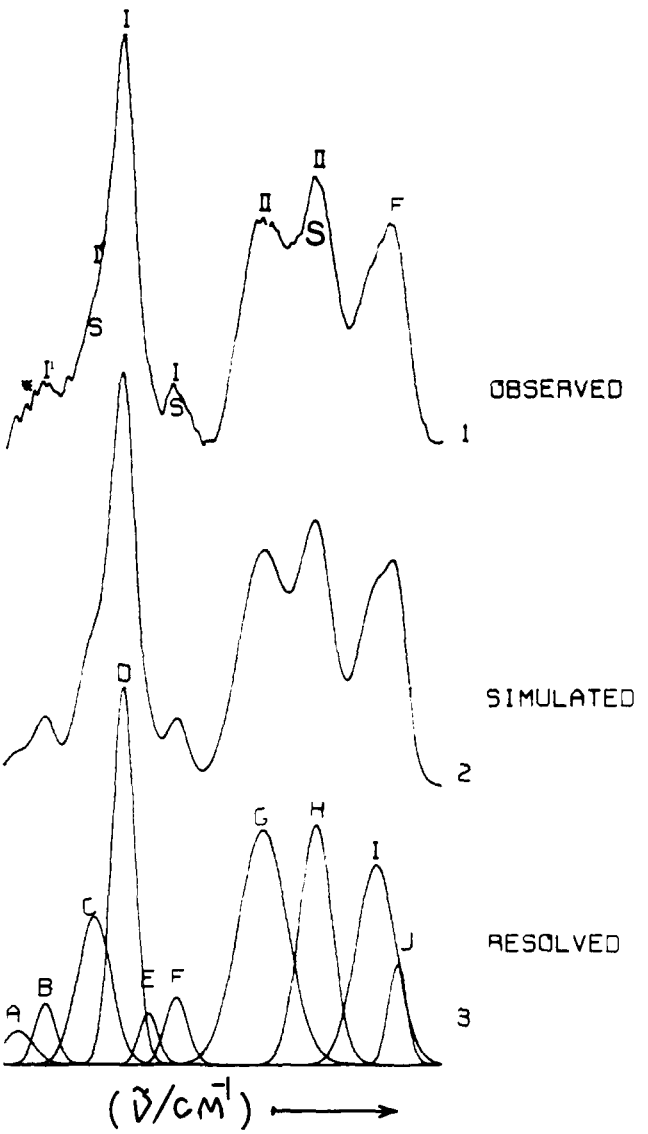

Figure 9. Observed, computer-simulated, and curve-resolved far-IR spectra of $Ca_{21.5}Y$. Note that the asterisks denote proposed IR-active symmetric metal cation vibrations (see text).

where C_B is the Brodskii constant, C is the Badger constant, and α is the O–M̂–O bond angle for a particular cation site. The ratio of C_B for different sites (e.g., I and I′) can therefore be written as

$$\frac{C_B(I)}{C_B(I')} = \frac{C(I)[1 - \cos \alpha(I)]^{1/2}}{C(I')[1 - \cos \alpha(I')]^{1/2}}$$

Using this equation, we can therefore determine the ratio of the Badger constants for different cation sites. Assuming that the ratio of these constants will be invariant for a group of similar molecules, we can use it to predict the O–M̂–O angles for a variety of ion-exchanged faujasites. In the equation above, and its partners for sites II and III, we use the experimentally observed vibrational frequencies of $Ni^{2+}Y$ to give $C_B(I)/C_B(I')$ and the bond angles quoted by Gallezot et al.[23] for a dehydrated $Ni_{10}Na_{31}H_5Y$ sample ($\alpha(I) = 90°$, $\alpha(I') = 105°$, $\alpha(III'') = 140°$ (calculated)). Thereby $C(I)/C(I') = 1.11$ and $C(I)/C(III'') = 1.35$. These values predict that for $Cu^{2+}Y$, the O–M̂–O angles for sites I′ and III″ are 116.7° and 131.2°, respectively, assuming $\alpha(I) = 90°$. The X-ray value determined for $\alpha(I')$ is 115.9°[27] and the site III″ angle is not known. However, a calculation of the type described earlier for site III″ cations yielded 139.9°.

Angular information of this type is important in terms of gaining insight into the accessibility of threefold metal cation sites in the α and β cages, and particularly in terms of site III″ cations, where X-ray analyses fail, it could be generally applicable.

A Cautionary Note

In the intensity analyses of the E modes of the three-coordinate sites, I′ and II, it is important to recognize that the A_1, symmetric metal cation vibrational mode *is actually IR-active.* It is therefore pertinent to inquire into the magnitude of the IR-integrated intensity of the A_1 mode relative to the E-type asymmetric metal

LINE	WIDTH	INTENSITY	UNITS	AREA	%AREA
A	20.13	66	4136.93	63	3.7
B	16.66	168	3978.92	133	7.9
C	19.64	248	3816.20	231	13.8
D	24.92	241	3576.05	285	17.0
E	16.66	340	3363.31	268	16.0
F	16.17	214	3203.75	165	9.8
G	15.84	59	3052.25	44	2.6
H	36.30	279	2931.37	488	28.7

TOTAL AREA = 26744

RMS ERROR = 2.62

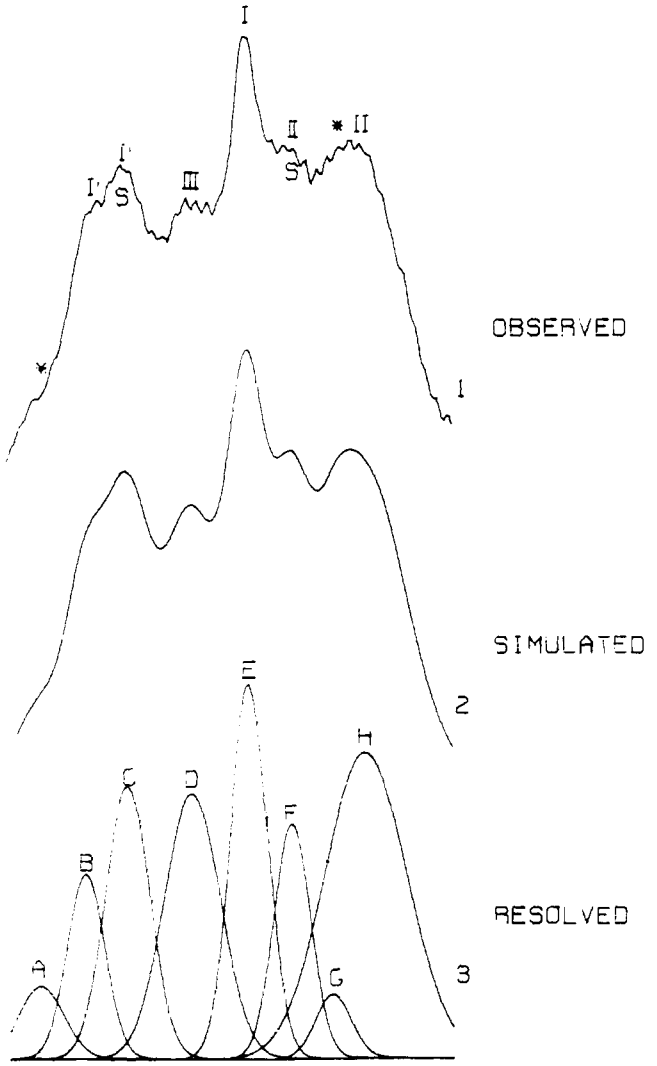

Figure 10. Observed, computer-simulated, and curve-resolved far-IR spectra of $Mn_{18.3}Y$. Note that the asterisks denote proposed IR-active symmetric metal cation vibrations (see text).

LINE	WIDTH	INTENSITY	UNITS	AREA	%AREA
A	15.60	116	125.29	122	7.9
B	27.85	182	133.38	279	17.4
C	16.23	125	144.38	199	9.9
D	22.92	267	156.80	683	26.8
E	23.88	238	166.54	521	22.2
F	24.25	193	174.54	462	25.5

TOTAL AREA = 1796

RMS ERROR = 2.61

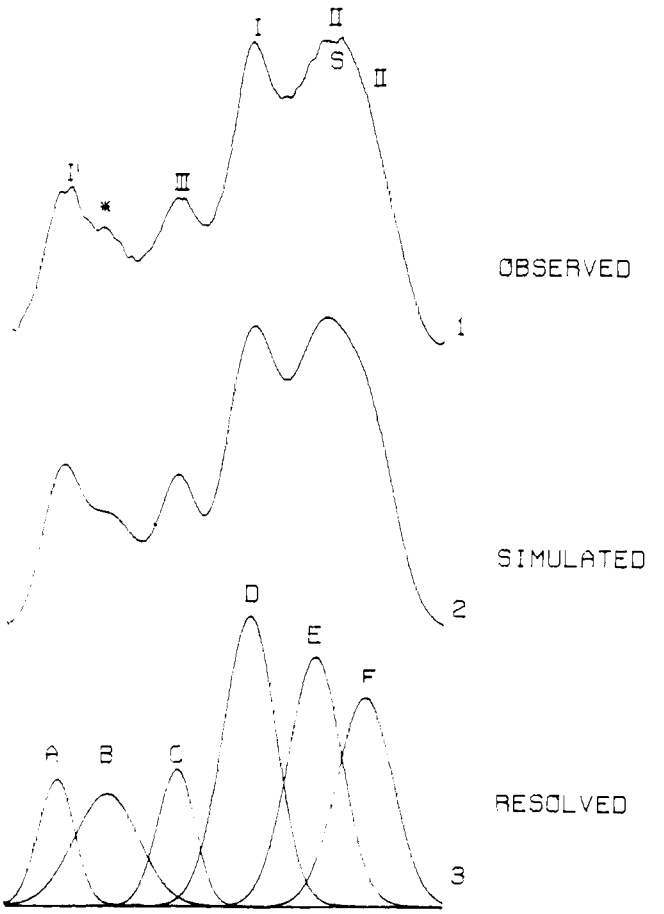

Figure 11. Observed, computer-simulated, and curve-resolved far-IR spectra of $Co_{14}Y$. Note that the asterisks denote proposed IR active symmetric metal cation vibrations (see text).

cation vibrational counterpart. An insight into this question can be gained by employing a similar transition bond dipole moment approximation to the A_1 and E modes of the C_{3v} $M^{q+}O_3$ site I′ or II "quasimolecule" described earlier. The relevant symmetry coordinates are

$$S_{A1} = (1/3)^{1/2}(\Delta R_1 + \Delta R_2 + \Delta R_3)$$

$$S_E = (1/2)^{1/2}(\Delta R_2 - \Delta R_3)$$

which leads to the respective transition bond dipole moment vectors and **G**-matrix elements shown below.

	$\left(\frac{\partial \vec{\mu}_y}{\partial S_k}\right)$	$\left(\frac{\partial \vec{\mu}_z}{\partial S_k}\right)$	$G_{k'k''}$
site I′; A_1		$(3)^{1/2}\cos\theta'$	$\mu_O + \mu_M(1 + 2\cos\alpha')$
site I′; E	$(3/2)^{1/2}\sin\theta'$		$\mu_O + \mu_M(1 - \cos\alpha')$

Keeping in mind the 1:2 weighting of the IR intensities originating from the single and double degeneracies of the A_1 and E modes, respectively, one arrives at the expression for the ratio of the intensities of the symmetric A_1 to the asymmetric E metal cation vibrational modes, namely

$$\frac{I_{A_1}(I')}{I_E(I')} = \left[\frac{3 - 4\sin^2\alpha'/2}{4\sin^2\alpha'/2}\right]\left[\frac{\mu_O + \mu_M(1 + 2\cos\alpha')}{\mu_O + \mu_M(1 - \cos\alpha')}\right]$$

This expression should apply equally well to any three-coordinate $M^{q+}O_3$ cation site. This analytical intensity ratio is represented graphically in Figure 13 for $\alpha' = 60°-120°$ for Ca^{2+} through to Zn^{2+}. The spread in I_{A_1}/I_E values between the Ca^{2+} and Zn^{2+} extreme cases is a maximum at about 10% for very small α' values around 60° and diminishes to zero at 90°.

These data indicate that for α' angles smaller than 100°, there exists the opportunity to observe significant IR intensity in the symmetrical metal cation mode of C_{3v} sites I′ and II.

By scanning the X-ray crystallographic literature for metal zeolites containing such C_{3v} $M^{q+}O_3$ sites,[8] one finds that the angle α' tends to fall in the range 105°–116°, implying values of 0.161–0.032, respectively, for the corresponding I_{A_1}/I_E ratio. This first approximation analysis of the order of magnitude expected

Table III. Observed and Calculated Metal Cation Far-IR Integrated Intensities and X-ray Crystallographically Determined Metal Cation Occupation Numbers for Sites I, I′, and II in Faujasite Zeolites

	far-IR intensity ratios						obsd X-ray cation site pop[a]			calcd G-matrix correction term $^3/_2[(\mu_O + 2\mu_M)/(\mu_O + \mu_M)]$
	calcd			obsd						
	SI/SI′	SI/SII	SI′/SII	SI/SI′	SI/SII	SI′/SII	NI/NI′	NI/NII	NI′/NII	
$Na_{56}Y$[a]	0.836	0.537	0.640	0.760	0.302	0.397	0.395	0.254	0.640	2.116
$Na_{56}Y$[b]	1.181	0.554	0.469	0.760	0.302	0.397	0.558	0.262	0.469	2.116
$Na_{86}X$	0.711	0.155	0.218	0.854	0.222	0.254	0.336	0.070	0.218	2.116
$Ca_{21.5}Y$	10.527	2.400	0.228	7.042	0.748	0.106	5.460	1.245	0.228	1.928
$Mn_{18.3}Y$	3.015	0.783	0.259	2.015	0.558	0.277	1.640	0.426	0.259	1.838
$Co_{14}Y$	8.920			3.400			4.900			1.820
$Cu_{13.2}Y$	0.600			0.580			0.333			1.802

[a] The quoted cation site populations are taken from the following references. $Na_{57}Y$: Eulenberger, G. R.; Shoemaker, D. F.; Keil, J. G. *J. Phys. Chem.* **1967**, *71*, 1812. [b] $Na_{57}Y$: Mortier, W. J., den Bossche, E. V.; Uytterhoeven, J. B. *Zeolites* **1984**, *4*, 41. $Na_{81}X$: Hseu, T. Ph.D. Thesis, University of Michigan, Ann Arbor, 1984. $Ca_{27}Y$: Bennett, J. M.; Smith, J. V.; *Mater. Res. Bull.* **1968**, *3*, 633. $Mn_{19.3}Y$: Pearce, J. R.; Mortier, W. J.; Uytterhoeven, J. B. *J. Chem. Soc., Faraday Trans.* **1979**, *75*, 1395. $Co_{14}Y$: Gallezot, P.; Imelik, B. *J. Chim. Phys. Phys.—Chim. Biol.* **1974**, *71*, 155. $Cu_{16}Y$: Gallezot, P.; Ben Tarrit, Y.; Imelik, B. *J. Catal.* **1972**, *26*, 295.

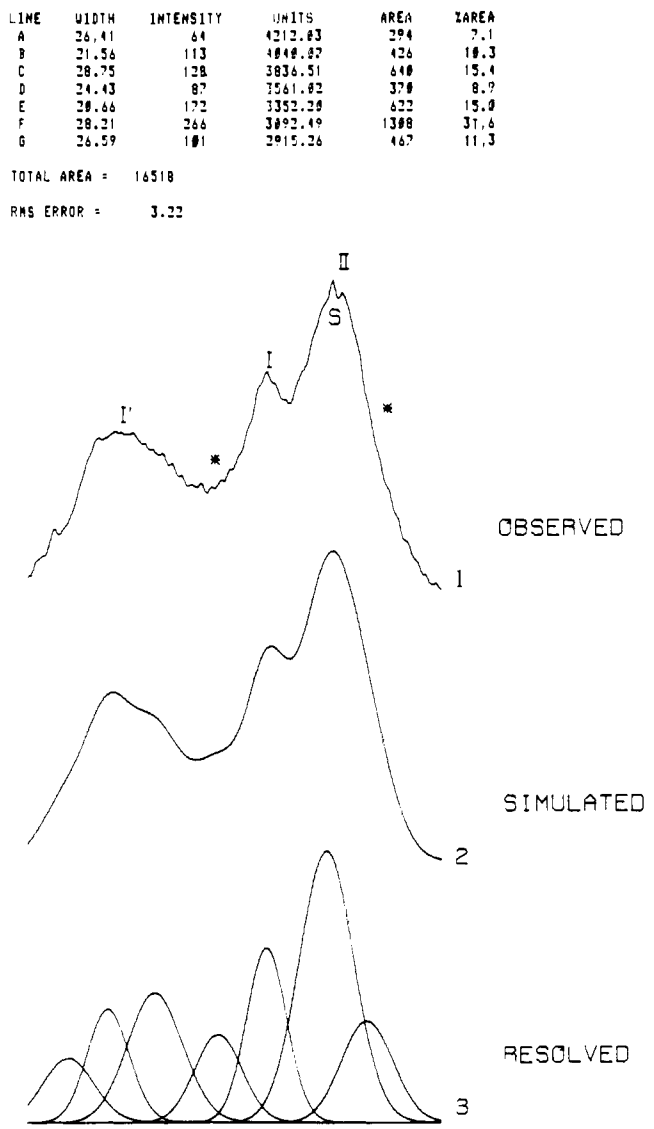

Figure 12. Observed, computer-simulated, and curve-resolved far-IR spectra of $Cu_{13.2}Y$. Note that the asterisks denote proposed IR-active symmetric metal cation vibrations (see text).

for the I_{A_1}/I_E ratios for three-coordinate C_{3v} $M^{q+}O_3$ sites alerts one to the possibility that unresolved shoulders or weak absorptions in the far-IR spectra of metal ion-exchanged zeolites containing these sites, which cannot be satisfactorily assigned to the anticipated asymmetric metal cation site modes, might well be ascribable to their IR-active symmetric partners. In the particular cases constituting the present study, we have in fact resorted to

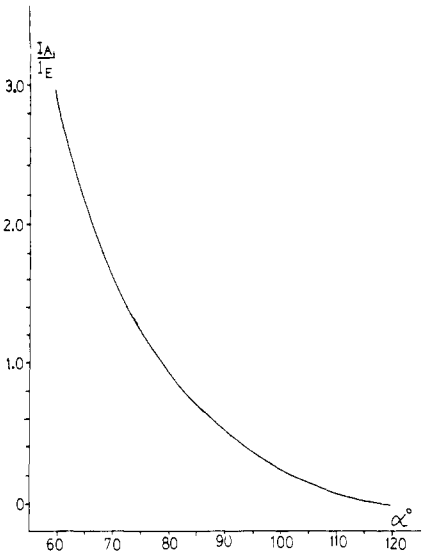

Figure 13. Graphical representation of the intensity expression

$$\frac{I_{A_1}(I')}{I_E(I')} = \frac{(3 - 4\sin^2\alpha'/2)(\mu_O + \mu_M[1 + 2\cos\alpha'])}{(4\sin^2\alpha'/2)(\mu_O + \mu_M[1 - \cos\alpha'])}$$

as a function of α' from 60° to 120°.

assigning unexplained bands (see asterisked bands in Figures 7–13) to just these kinds of A_1 symmetric $M^{q+}O_3$ metal cation vibrations.

In this context, the zeolites $Na_{56}Y$ and $Na_{86}X$ containing only Na^+ cations provide an opportunity for examining this idea further. By inspection of Figures 7 and 8, one notices the presence of weak, high-frequency asterisked shoulders on the asymmetric E-type ν_{NaO_3} modes for both C_{3v} sites II and I″. Could these be the corresponding symmetric A_1-type ν_{NaO_3} vibrations? An insight into this question can be obtained by calculating the frequencies of the A_1Na^+ cation vibrations for these sites based on the frequencies of the observed E-type modes, using the local molecule approximation and the respective **G**- and **F**-matrix elements for these sites described earlier in this paper.

This approach yields the frequency ratio

$$\frac{\nu_{A_1}^2}{\nu_E^2} = \left[\frac{k_r + 2k_{rr}}{k_r - k_{rr}}\right]\left[\frac{\mu_O + \mu_M[1 + 2\cos\alpha]}{\mu_O + \mu_M[1 - \cos\alpha]}\right]$$

By varying the O–M̂–O angle α in the range 90°–120° and the stretch–stretch interaction force constant k_{rr} from +0.25 to −0.10 of the value of the primary bond stretching force constant k_r, one discovers that for both site II and I′, quite acceptable frequency fits for the intense E Na^+ cation modes and the associated weaker asterisked A_1 modes can be found for $k_{rr} = 0.1k_r$ and $\alpha = 90°$, as well as $k_{rr} = 0.25k_r$ and $\alpha = 105°$, yielding $k_r^{II} = 0.22$–0.24

and $k_r^{I'} = 0.072$–0.079 mdyne Å^{-1}, respectively. This agreement lends some credance to the proposition that the low-intensity asterisked bands in the far-IR spectra of $Na_{56}Y$ and $Na_{86}X$ may be associated with the symmetrical counterparts of the main, asymmetric site II and I′ E-type Na^+ cation vibrations. Raman experiments are underway in our laboratory to investigate this idea further.

Clearly similar ideas to those expounded for sites I′ and II apply to site III cation modes. For example, in the case of site III″ cations, the local symmetry of the site is C_s and is expected to display 2A′ + A″ ν_{MO_3} cation modes, of which the asymmetric A″ is likely to be the most intense but with some measureable IR activity from at least one of the A′ symmetric modes. Finally one should note that "second-order" intensity effects relating, for example, to Jahn–Teller cation site distortions for transition-metal 2+ ions, reductions in site symmetry orginating from the Si/Al distribution in the zeolite lattice, and small deviations from ideal site symmetries (e.g., site I, $O_h \rightarrow D_{3d}$), can give rise to slight IR activity to cation modes which would normally be IR silent.

Conclusions. This paper demonstrates that far-infrared spectroscopy is an extremely sensitive direct probe of the cation locations in faujasite zeolites. It is an extremely powerful partner to X-ray diffraction techniques and succeeds in locating previously unidentified cations. In terms of a fuller understanding of the catalytic behavior of zeolites, this is clearly of pivotal importance. The main conclusions of this paper can be summarized as follows:

1. A local molecule **GF**-matrix approximation for computing the vibrational frequencies of cation modes for metal faujasite zeolites can satisfactorily explain the frequency ordering I > I′ > III′ for alkali-metal 1+ and I > III″ > I′ for transition-metal 2+ ion-exchanged faujasite.

2. Site III transition-metal ion vibrations occur at much higher frequencies than one would predict by using the Brodskii approach and site III frequencies for alkali-metal zeolites. Hence the assignment of III″ for the former and III′ for the latter is favored.

3. Far-infrared spectroscopy can identify cation occupancy of sites that have previously remained unnoticed.

4. From the data gathered in this first study, one feels optimistic that the transition bond dipole moment approach to the analysis of the far-IR intensities of metal cation vibrational modes in faujasites carries considerable potential as a valuable adjunct to the Brodskii or **GF**-frequency method for assigning metal cation IR bands and site locations in the zeolite framework. Furthermore, the intensity method offers new opportunities to establish actual site populations of exchangeable metal cations in the zeolite, thereby complimenting X-ray crystallographic techniques.

5. A local molecule **GF**-matrix and transition bond dipole moment analysis of the expected frequencies and intensities of IR-active "symmetrical" metal cation vibrations of three-coordinate sites (in relation to their "asymmetrical" counterparts) alerts one to the realization that weak bands and unexplained absorptions might have their origin in just these kinds of symmetrical modes and therefore they should not be neglected when evaluating the far-IR spectra of metal ion-exchanged zeolites.

However, numerous new and fascinating questions have been raised by this work, and many problems remain which will require close attention in future studies of metal ion-exchanged zeolites.

Acknowledgment. The financial assistance of the Natural Sciences and Engineering Research Council of Canada's Strategic Grants Programme and the Connaught Foundation of the University of Toronto is greatly appreciated. We are also indebted to Drs. Edith Flanigen (Union Carbide) and Paul Kasai (IBM) for various ultrahigh purity zeolites and to Kate Helwig for her invaluable technical assistance with the preparation of zeolite samples.

Identification of Proton NMR Signals from the Metal Ligands in Cadmium-Substituted Plastocyanin via Two-Dimensional Multiple-Quantum Detection in the Absence of Explicitly Resolved ^1H–^{113}Cd Coupling

David H. Live,*[†,‡] Christopher L. Kojiro,[§] David Cowburn,[†] and John L. Markley*[§,⊥]

Contribution from The Rockefeller University, New York, New York 10021, and Department of Chemistry, Purdue University, West Lafayette, Indiana 47907. *Received January 2, 1985*

Abstract: Two-dimensional (2D) proton-detected heteronuclear $^1H\{^{113}Cd\}$ multiple-quantum (HMQ) NMR spectroscopy of ^{113}Cd-substituted plastocyanin from spinach (*Spinacia oleracea*) yielded signals from the four amino acid side chains ligated to the metal. HMQ coherences over four bonds were observed with the metal ligands histidine-37 and histidine-87. Assignments of signals from the metal ligands, cysteine-84 C_β–$^1H_2$ and methionine-92 C_ϵ–$^1H_3$, are proposed. HMQ signals were observed in the absence of resolved ^1H–^{113}Cd coupling. The 2D HMQ method should be useful for identifying ^1H NMR peaks from metal ligands in metalloproteins.

Identification of resonances from the metal ligand residues represents an essential step in characterizing metalloproteins by NMR spectroscopy. ^1H NMR assignments for resonances from the two histidine and single methionine ligands in the "blue copper" protein plastocyanin have been reported.[1-3] These assignments in the Cu(I) form of the protein have been based on comparisons with spectra of the Cu(II) protein in which signals from groups close to the metal exhibit characteristic paramagnetic broadening.

[†] The Rockefeller University.
[‡] Present address: Jet Propulsion Laboratory, California Institute of Technology, Pasadena, CA 91109.
[§] Purdue University.
[⊥] Permanent address: Department of Biochemistry, University of Wisconsin–Madison, Madison, WI 53706.

(1) Markley, J. L.; Ulrich, E. L.; Berg, S. P.; Krogmann, D. W. *Biochemistry* **1975**, *14*, 4428–4433.
(2) Freeman, H. C.; Norris, V. A.; Ramshaw, J. A. M.; Wright, P. E. *FEBS Lett.* **1978**, *86*, 131–135.
(3) Cookson, D. J.; Hayes, M. T.; Wright, P. E. *Biochim. Biophys. Acta* **1980**, *591*, 162–176.

0002-7863/85/1507-3043$01.50/0